Breakup and neutron-transfer effects on ^{6}He + ^{206}Pb elastic scattering below the Coulomb barrier

Ł. Standyło,[1] L. Acosta,[2] C. Angulo,[3] R. Berjillos,[2] J. A. Duenas,[2] M. S. Golovkov,[4] N. Keeley,[5,*] T. Keutgen,[3] I. Martel,[2] M. Mazzocco,[6] F. Perez-Bernal,[2] A. M. Sánchez-Benítez,[2] C. Signorini,[6] M. Romoli,[7] K. Rusek,[1,5] and R. Wolski[4,8]

[1]*Heavy Ion Laboratory, University of Warsaw, Pasteura 5A, PL 02-093 Warsaw, Poland*
[2]*Departamento de Física Aplicada, Universidad de Huelva, E-21071 Huelva, Spain*
[3]*Centre de Recherches du Cyclotron, Université Catholique de Louvain, B-1348 Louvain-la-Neuve, Belgium*
[4]*Flerov Laboratory of Nuclear Reactions, JINR, 141980 Dubna, Russia*
[5]*National Centre for Nuclear Research, ul. Andrzeja Sołtana 7, 05-400 Otwock, Poland*
[6]*INFN–Laboratori Nazionali di Legnaro, Viale dell' Universitá 2, 35020 Legnaro, Italy*
[7]*Istituto Nazionale di Fisica Nucleare, I-80126 Napoli, Italy*
[8]*The Henryk Niewodniczański Institute of Nuclear Physics PAN, 31-342 Kraków, Poland*

(Received 10 May 2013; published 4 June 2013)

The elastic scattering and inclusive α-particle yield for the ^{6}He + ^{206}Pb system at an incident energy of 18 MeV, just below the nominal Coulomb barrier, have been measured. The α-particle yield at forward angles is also reported. The data are analyzed by means of continuum-discretized coupled-channels, distorted wave Born approximation, and coupled reaction channels calculations. Couplings to the one-neutron- and two-neutron-transfer reactions are found to be able to account for most of the absorption in the entrance channel.

DOI: 10.1103/PhysRevC.87.064603 PACS number(s): 25.60.Bx, 25.60.Dz, 25.70.Bc, 24.10.Eq

I. INTRODUCTION

The radioactive nucleus ^{6}He has a three-body $\alpha + n + n$ structure with an extended neutron distribution or halo. The scattering and reactions of ^{6}He are therefore of considerable interest since experiments may demonstrate a sensitivity to this underlying structure. In addition, its threshold against $^{6}\text{He} \rightarrow \alpha + n + n$ breakup is less than 1 MeV and this weakly bound nature can also significantly affect the dynamics of the collision. Here we report a measurement of the elastic scattering and inclusive α-particle production in the ^{6}He + ^{206}Pb system at an incident energy of 18 MeV, just below the nominal Coulomb barrier. Similar measurements of elastic scattering in the ^{6}He + ^{208}Pb system have been reported at incident energies of 14, 16, 18, 22 [1], and 27 MeV [2] and for the backward angle ($\theta > 120^{\circ}$) α-particle production at 14, 16, 18, and 22 MeV [3]. The present data extend the angular coverage of the α-particle production cross section angular distribution to more forward angles, into the region where Coulomb breakup of ^{6}He via the $^{6}\text{He} \rightarrow \alpha + n + n$ process is expected to dominate over one-neutron ($1n$) and two-neutron ($2n$) stripping in the reaction mechanism. The data reported here thus provide an opportunity for testing models of the breakup of ^{6}He as well as for probing the effects of $1n$ and $2n$ stripping.

The main motivation behind the choice of a ^{206}Pb target in the present experiment was to repeat and extend previous measurements of the near- and sub-barrier ^{6}He + ^{206}Pb fusion excitation function [4] with better beam energy resolution. (These results, taken simultaneously with the elastic scattering and α-particle production cross section measurements described here have been reported elsewhere [5].) Nevertheless, while the breakup cross section should not differ significantly for a ^{208}Pb or a ^{206}Pb target, the target being essentially an inert spectator in the usual breakup process, the use of a ^{206}Pb target does allow for an interesting check of the influence of target structure on $1n$ stripping; while we do not anticipate much difference for $2n$ stripping because of the preferential population of high-lying states close to the $2n$ emission threshold due to the large positive Q value for the (^{6}He,^{4}He) transfer process, $1n$ stripping will populate relatively low-lying states where differences in the single-particle structure of ^{207}Pb and ^{209}Pb may play a role. If such differences are important they should be observable in the α-particle production angular distribution and/or the coupling influence of $1n$ stripping on elastic scattering.

This paper is divided into the following sections: in Sec. II the experimental method is described. Sections III and IV describe calculations probing the effect of breakup and $1n$ and $2n$ stripping, respectively. Finally, Sec. V contains a summary and conclusions.

II. EXPERIMENTAL METHOD

The experiment was performed at the Cyclotron Research Centre in Louvain-la-Neuve, Belgium. The radioactive ^{6}He beam was produced via the $^{7}\text{Li}(p, 2p)^{6}\text{He}$ reaction using a LiF powder target contained in a graphite holder [6]. A high-current 30-MeV proton beam from the Cyclone-30 cyclotron was used to produce the secondary ^{6}He beam, which was subsequently ionized in an electron cyclotron resonance (ECR) ion source, then separated and postaccelerated in the Cyclone-110 cyclotron. The final ^{6}He beam had a laboratory energy of 18 MeV with a charge state of 1^{+} and an average intensity of about 1.6×10^{7} ions per second. Two targets were used: a scattering target of ^{206}Pb metal (97%) with a thickness of 0.5 mg/cm^{2} evaporated onto a 0.042 mg/cm^{2} carbon foil and an activation stack of targets formed by evaporating ^{206}PbS compound (94%) onto Ti foils used for the fusion measurement reported in Ref. [5]. Full details are given in Ref. [5].

*keeley@fuw.edu.pl

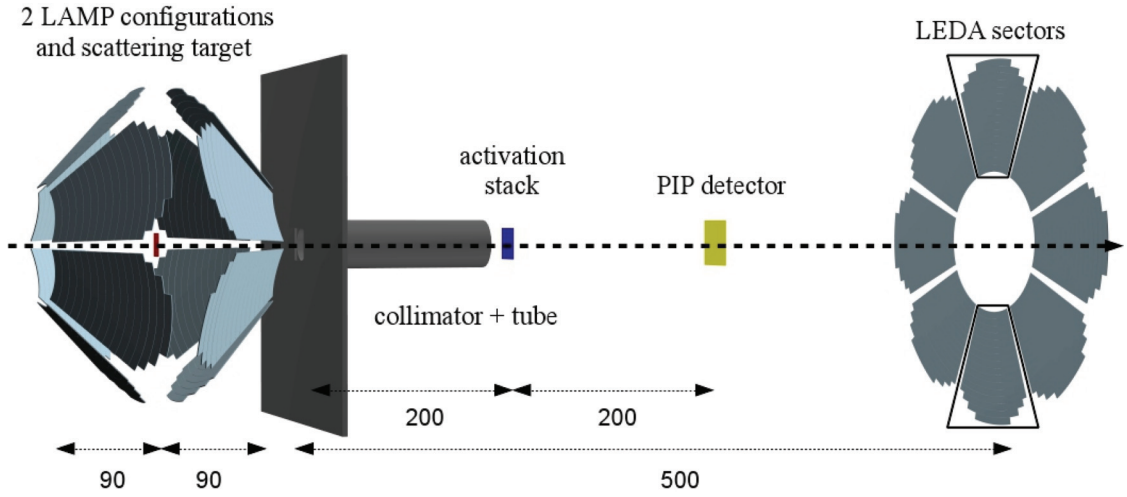

FIG. 1. (Color online) Schematic of the experimental setup. All distances are in millimeters.

The experimental setup is shown in Fig. 1. Elastically scattered particles and reaction products were measured in a detection system consisting of two Louvain Edinburgh Detector Array (LEDA) silicon detector arrays of five sectors each arranged in a six-sided cone, the so-called "LAMP" configuration, covering average forward scattering angles from 25° to 70° and backward angles from 105° to 165°. Each sector consisted of 16 strips with a thickness of 300 μm, an angular coverage of 42°, and a total active area of 45.9 cm^2. Two further LEDA sectors in an annular configuration with each sector normal to the beam direction were placed downstream of the activation stack to monitor the total projectile flux incident on the stack targets. The master trigger was set as a common OR; thus all events in any of the detectors were registered. A 10-mm-diameter collimator was placed between the scattering chamber and the activation stack to prevent the LAMP detectors registering back-scattered products from the activation stack. Further details of the experimental setup are given in Ref. [5].

The experiment did not employ detector telescopes so that particle identification via the ΔE-E method was not possible. However, previous experiments [1,7] with ^{6}He + ^{208}Pb found that the only charged-particle reaction products of importance were ^{6}He and α particles. In addition to a sharp peak corresponding to elastically scattered ^{6}He ions a large, broad peak was observed in the energy spectra, ascribed to α particles produced by the $^6\mathrm{He} \rightarrow \alpha + n + n$ breakup and the $1n$- and $2n$-stripping reactions (see Figs. 2 and 3). Energy calibration of the silicon detectors was performed using a triple-α source.

The presence of a large (about 11% of the total number of counts) background at forward angles was the main problem in extracting the elastic scattering and α-particle production yields. At forward angles the elastic peak varies in shape from a form similar to a Dirac delta function at the smallest angles to a wider form more like a Bragg peak at larger angles. It was therefore fitted using a combined Gaussian + Lorentz function, which well describes this shape. At forward angles the data analysis procedure adopted was to fit the background and the elastic peak as accurately as possible, with the α-particle yield being obtained by subtracting the fitted elastic peak and background events from the total number of events in the spectrum (see Fig. 2). At backward angles the procedure was much simpler. Both peaks, elastic scattering and α particle, were fitted using a Gaussian shape and the background under the fit, which was much smaller (about 6%) compared to forward angles, was subtracted (see Fig. 3). In addition to the elastic scattering and reaction events, products from the elastic scattering of ^{6}He from the carbon backing of the target, along with a small number of events from the interaction of the beam with the aluminum target holder, were also observed.

Figure 4 plots the number of counts as a function of laboratory energy versus laboratory angle. A clear group of counts at an energy of about 14 MeV (the ringed region on Fig. 4 centered at $\theta_{\mathrm{lab}} = 60°$) can be noted. These can only be explained as coming from direct $^6\mathrm{He} + n + n$ breakup, although based on this hypothesis they should have an energy of about 4/6 that of the beam, i.e., about 12 MeV (with the kinematic curve for this reaction being plotted on Fig. 4 as

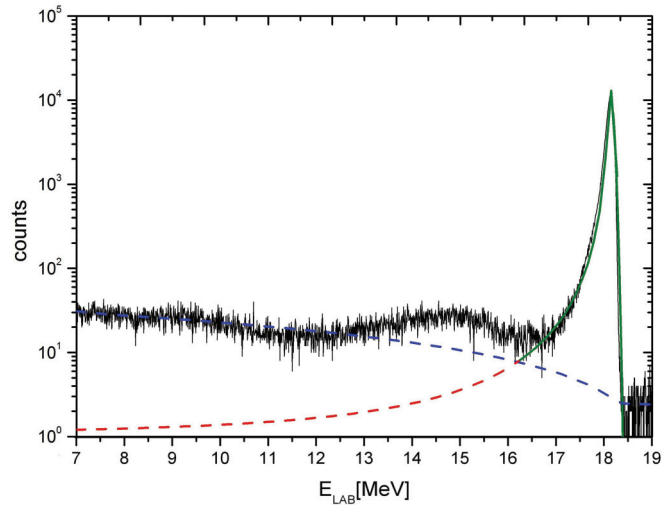

FIG. 2. (Color online) Energy spectrum from a forward LAMP detector at $\theta_{\mathrm{lab}} = 48.05°$. In addition to the large, sharp ^{6}He elastic peak, a small, flat α-particle peak was also observed. Note the logarithmic counts scale.

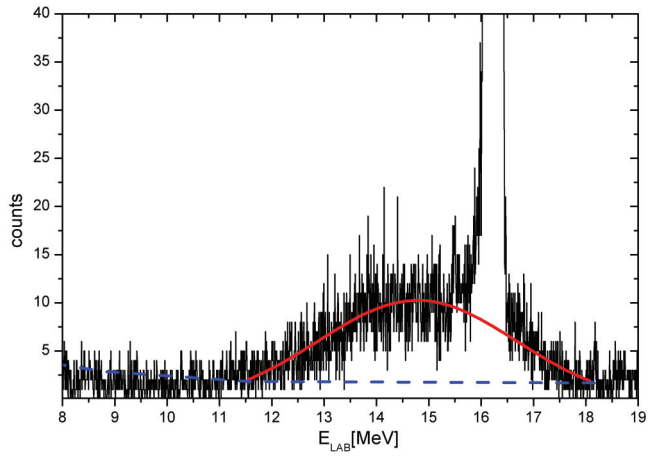

FIG. 3. (Color online) Energy spectrum from a backward LAMP detector at $\theta_{\rm lab} = 154.9^\circ$. The elastic peak sits on top of the flat Gaussian-shaped α peak. Note the linear counts scale.

the long-dashed curve). The apparent discrepancy may be explained as due to Coulomb postacceleration of the α particles after breakup. At $\theta_{\rm lab} = 60^\circ$ the shift is about 2.3 MeV. From this we may infer that breakup takes place at a distance from the target of about 34 fm at this angle. The discrepancy between the kinematic prediction and the centroid of the α peak increases with increasing scattering angle. This could be interpreted as a signature of different reaction mechanisms. At more backward angles the α particles could come from $1n$ ($Q_{gg} = +4.87$ MeV) and $2n$ ($Q_{gg} = +13.1$ MeV) transfer reactions rather than from ^{6}He breakup. Since the Coulomb

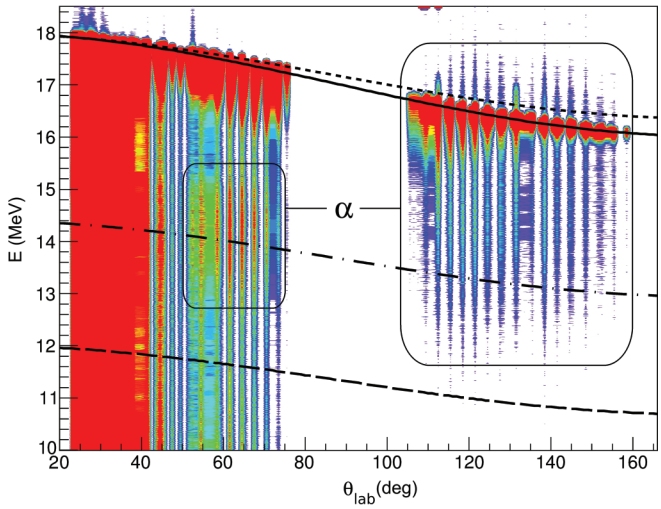

FIG. 4. (Color online) Kinematics diagram of laboratory energy vs laboratory angle. The solid line denotes the calculated kinematic curve for the ^{6}He + ^{206}Pb elastic scattering and the long-dashed curve that for α particles at 4/6 the beam energy produced in the ^{6}He $\rightarrow \alpha + n + n$ breakup reaction. The short-dashed and dot-dashed lines denote the kinematic curves for $2n$ and $1n$ transfer, respectively, both plotted for "effective" Q values of 0.0 MeV (see text). (The energy scale of the $1n$-transfer curve was multiplied by 4/5 because the α particles from the decay of the ^{5}He were detected rather than the ^{5}He itself.) The regions where α particles were actually observed are ringed.

postacceleration of the ^{5}He from $1n$ transfer is much weaker than the postacceleration of α particles from ^{6}He breakup and the optimum Q value of the neutron-transfer reaction should be close to zero, the centroid of the α peak at mid-range scattering angles (where $1n$ transfer is expected to dominate) is closer to the kinematic curve for this process, plotted for an "effective" Q value of 0.0 MeV (dot-dashed curve in Fig. 4). At the most backward angles the centroid of the α peak is at a lower energy than expected from the $2n$-transfer kinematics (short-dashed curve, again plotted for an effective Q value of 0.0 MeV), which suggests that in this angular region the α particles arise due to $2n$ transfer to states in the $2n + ^{206}$Pb continuum located a few MeV above the $2n + ^{206}$Pb threshold of ^{208}Pb.

Elastic scattering data are very sensitive to beam misalignment at the target, especially at sub-barrier energies. Any misalignment was corrected for using a standard method described in Ref. [8], based on the fact that Rutherford scattering of charged particles from a nucleus with charge Ze has cylindrical symmetry about the beam axis [9]. The difference between the measured and calculated elastic yields in the angular region where the elastic scattering corresponds to Rutherford scattering was minimized and the effective position of the beam spot thus obtained was used to introduce a correction in the elastic yields due to the variation in the solid angles [7].

The angular distribution of the elastic scattering differential cross section was obtained from the relation [10]

$$\frac{\sigma_{\rm el}(\theta_i)}{\sigma_{\rm Ruth}(\theta_i)} = \frac{N(i)}{\Delta\Omega(i)^{\rm lab}} \frac{1}{K} F(i), \tag{1}$$

where K is a normalization constant, $N(i)$ is the number of elastic events in detector strip i, $\Delta\Omega(i)^{\rm lab}$ is the solid angle for each strip calculated according to the method described in Ref. [9], and $F(i)$ accounts for the correction due to beam misalignment. The constant $K = 267.68$ was determined from the assumption that for small scattering angles the elastic scattering cross section is equal to the Rutherford cross section. The cross section for the α-particle yield was obtained from the ratio of α-particle to elastic scattering events, $N_\alpha(\theta_i)/N_{\rm el}(\theta_i)$, and the elastic scattering differential cross section using the expression

$$\sigma_\alpha(\theta_i) = \frac{N_\alpha(\theta_i)}{N_{\rm el}(\theta_i)} \sigma_{\rm el}(\theta_i). \tag{2}$$

The statistical uncertainties in the α-particle cross section at forward angles are large since the number of elastic events is very large compared to the number of α events in this angular region.

III. BREAKUP EFFECT

In this section we investigate the influence of coupling to the breakup channels on ^{6}He + ^{206}Pb elastic scattering. One of the most effective means to calculate breakup of weakly bound projectiles is the continuum-discretized coupled-channels (CDCC) method. It has been used successfully to describe the breakup of ^{6}He in the field of different targets. The most realistic model of ^{6}He is as a three-body object, with an α-particle core and two neutrons forming a halo state. CDCC calculations

employing such a model, called "four-body CDCC," were used to analyze ^{6}He elastic scattering from a ^{208}Pb target at 22 MeV [11]. They gave a similar description of the experimental data to "three-body CDCC" results [12,13] based on a much simpler dineutron model of ^{6}He [14]. "Three-body CDCC" was used to analyze ^{6}He + ^{208}Pb elastic scattering at a range of energies from just below to just above the Coulomb barrier [15]. In order to have a direct comparison with these results we have performed similar "three-body CDCC" calculations. All calculations were carried out using the code FRESCO [16]. The α + dineutron wave functions of ^{6}He were calculated in a Woods-Saxon potential with geometry $R = 1.9$ fm and $a = 0.39$ fm [17]. The effective α + dineutron separation energy was set to 1.6 MeV, following the work of Ref. [14]. The continuum above the breakup threshold was discretized into equally spaced bins in momentum space. Details of the binning scheme may be found in Ref. [18]. The fragment-target optical potentials used to generate the diagonal and coupling potentials via Watanabe-type folding were adopted from previous studies [18,19]. For the dineutron + ^{208}Pb optical potential the deuteron potential of Ref. [20] was used and for α + ^{208}Pb the potential of Goldring *et al.* [21] was used.

The results of calculations for elastic scattering are plotted in Fig. 5. The effect of the breakup coupling is illustrated by the difference between the dotted and solid curves. The dotted curve presents the result of a calculation without any couplings—an optical model calculation with the "bare" potential, the diagonal potential in the entrance channel—while the solid curve denotes the result of a calculation including couplings to the 2^{+} resonant state of ^{6}He at $E_{ex} = 1.8$ MeV and the nonresonant continuum, including continuum-continuum couplings. The total breakup cross section emerging from this calculation is 151 mb and the total reaction cross section is 572 mb.

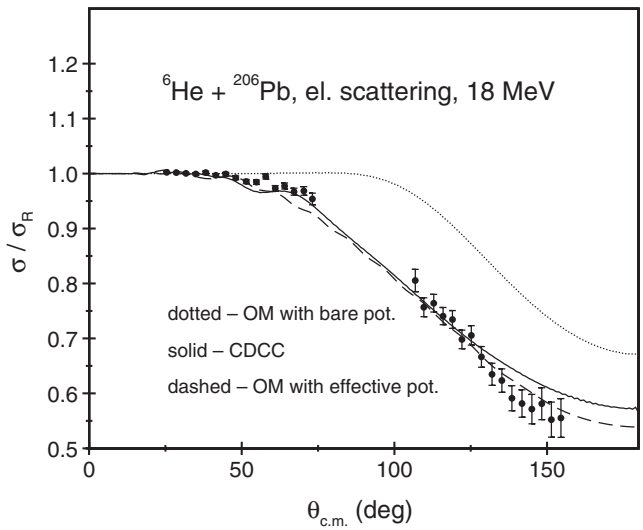

FIG. 5. Breakup effect on elastic scattering. The dotted curve shows the result of an optical model (no-coupling) calculation with the bare potential while the result of the CDCC calculation including couplings to the breakup channels is denoted by the solid curve. The dashed curve denotes the result of an optical model calculation with the effective potential (see text).

The agreement with the data is good, except for a slight overprediction at backward angles ($\theta_{c.m.} \geqslant 125^{\circ}$). In this respect the results are similar to those for a ^{208}Pb target at energies above the Coulomb barrier, 22 and 27 MeV [12,18], where similar calculations also reproduced the experimental data very well. However, for this lower energy the coupling effect is much more pronounced.

From the CDCC calculations one can extract so-called trivially equivalent L-dependent polarization potentials [22]. By taking the weighted mean value of these potentials an L-independent dynamic polarization potential (DPP) can be constructed [23]. If the DPP extracted in this way is a proper representation of the coupled-channel effects, an optical model calculation with the effective potential (the sum of the bare potential and the DPP) should reproduce the CDCC results. Such an effective potential was derived from the present CDCC calculation. While the result of an optical model calculation with this potential is not absolutely identical to the original CDCC result it is sufficiently close that we may consider the DPP to provide an adequate representation of the breakup coupling effect on the elastic scattering (see the dashed curve in Fig. 5).

IV. EFFECT OF NEUTRON-TRANSFER REACTIONS

In this section we examine the influence of coupling to $1n$- and $2n$-transfer reactions on elastic scattering. Distorted wave Born approximation (DWBA) calculations are initially made to establish realistic coupling strengths for these processes by a comparison with the inclusive α-particle production data. Coupled reaction channels (CRC) calculations are then performed to establish the coupling effect on the elastic scattering.

A. DWBA calculation of $1n$ transfer

According to the shell-model calculations of Ref. [24] the ground-state wave function of ^{6}He consists of $^{5}\mathrm{He}_{g.s.} + n(1p_{3/2})$ and $^{5}\mathrm{He}_{1exc.} + n(1p_{1/2})$ components, with spectroscopic amplitudes of 1.2648 and 0.8944, respectively. Spectroscopic factors for the $^{207}\mathrm{Pb} = {}^{206}\mathrm{Pb} + n$ overlaps were taken from the ^{206}Pb(d, p) studies of Moyer *et al.* [25]. In the present calculations, transfers to the single-particle states in the final nucleus at the following excitation energies were taken into account: 0.0, 2.73, 4.40, 4.64, 5.14, and 5.23 MeV. The potentials binding the neutron to the ^{5}He and ^{206}Pb cores were of Woods-Saxon shape with the standard geometry parameters: $R = 1.35 \times A^{1/3}$ fm and $a = 0.65$ fm.

In the entrance channel the effective optical potential—i.e., that including the effects of coupling to breakup channels as described in the previous section—was used. The potential in the exit channel was calculated by folding empirical n + ^{207}Pb and α + ^{207}Pb optical potentials with the wave function of the ^{5}He ground state. This wave function, in turn, was calculated using the method described in Ref. [26]. The global nucleon-nucleus potential of Ref. [27] was adopted for the n + ^{207}Pb optical potential while for α + ^{207}Pb the optical potential

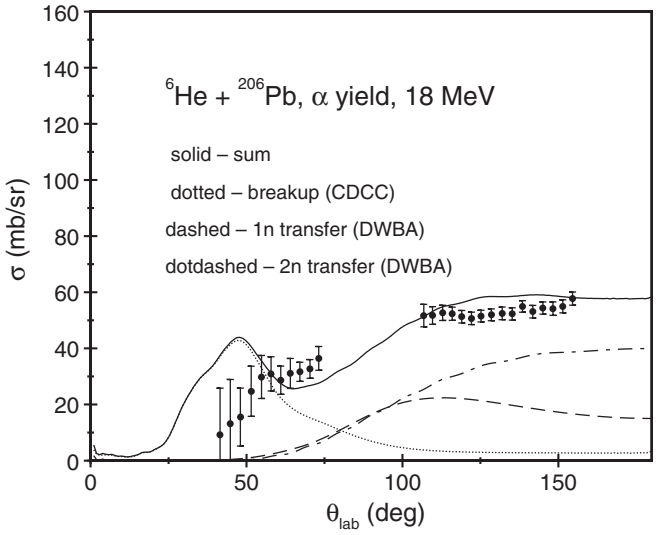

FIG. 6. Angular distribution (in the laboratory system) of the α particles emitted in the ^{6}He + ^{206}Pb reaction at 18 MeV. The solid curve represents the total calculated yield due to ^{6}He breakup (dotted curve), one-neutron transfer (dashed curve), and two-neutron transfer (dot-dashed curve). The transfer calculations were performed using the DWBA method.

used in the input to the CDCC calculations to generate the ^{6}He + ^{208}Pb interactions was employed [21].

The results of the DWBA calculations are plotted as the dashed curve in Fig. 6. The calculated $1n$-transfer cross section is 153 mb, a value comparable with the breakup cross section.

B. DWBA calculation of $2n$ transfer

A method to calculate $2n$ transfer from ^{6}He to the ^{210}Pb continuum was developed by Escrig *et al.* [3] and used to study the α-particle yield emitted in the ^{6}He + ^{208}Pb reaction at energies around the Coulomb barrier [12,15]. In general, the calculations slightly underestimated the number of measured α particles at backward angles.

In this work we have applied a more phenomenological approach. The Q value for the ^{206}Pb(^{6}He, α)^{208}Pb reaction is large and positive, $Q = 13.1$ MeV, and the $2n$ binding energy of ^{208}Pb is $S_{2n} = 14.1$ MeV. From the ^{6}He + ^{208}Pb experiments we have learnt that the optimum Q value for the $2n$-transfer process is zero or even slightly negative [12]. In other words, the transfer proceeds mainly to highly excited states in the final nucleus located around the binding energy. Thus, our DWBA calculations were performed for a fictitious dineutron state in ^{208}Pb placed at an excitation energy of 14.0 MeV. The quantum numbers of this state were set to $6S_0$ and the potential binding the dineutron to the ^{206}Pb core was of Woods-Saxon shape with geometry $R = 1.25 \times 206^{1/3}$ fm and $a = 0.65$ fm. For the ^{6}He = ^{4}He + ^2n overlap, the dineutron model used in the CDCC calculations was employed.

In the entrance channel the effective potential derived from the CDCC calculations (and already used in the $1n$-transfer calculations) was employed and in the exit channel the α + ^{208}Pb optical potential from the CDCC input was adopted [21]. The DWBA cross section was normalized to the experimental data in the following way. As mentioned above, the CDCC calculations yielded a total reaction cross section of 572 mb and a breakup cross section of 151 mb, thus leaving 421 mb for the other reaction channels. Subtracting the calculated $1n$-transfer cross section (153 mb) and the measured fusion cross section (48 mb [5]) and assuming that the only remaining process is $2n$ transfer, we normalized the DWBA $2n$-transfer cross section to the remaining 220 mb, obtaining a value for the normalization constant of $S = 6.1$. The result of this approach is plotted as the dot-dashed curve in Fig. 6. The results of the calculations were transformed from the c.m. frame to the laboratory frame in order to compare them with the experimental results.

While the transformation from c.m. to laboratory frame is straightforward for the $2n$ transfer, it is difficult for the other two processes. The breakup calculations produced an angular distribution of the excited ^{6}He where the c.m. angle is that of the α + dineutron system—the inelastically scattered "^{6}He" nucleus—and not the angle of the α particles detected in the experiment. In order to make a comparison with the experiment, the two angles were assumed to be the same. Under this assumption, the calculated cross section for ^{6}He breakup was transformed from the c.m. to the laboratory frame and the result is plotted as the dotted curve in Fig. 6. The transformation for the $1n$ transfer was made under the assumption that the angle of the emitted ^{5}He is identical with the angle of the α particle that is the product of its decay. The result is plotted as the dashed curve in Fig. 6.

The solid curve in Fig. 6 represents the sum of the three calculated processes. It overestimates the measured values at forward angles and also at angles around 125°. Here one should remember that the measurements at forward angles were difficult to make due to the large background. Nevertheless, even taking into account the very approximate transformation of the breakup calculations from the c.m. to the laboratory frame, the agreement between the data and the predictions is rather poor.

C. CRC calculations

In order to learn about the effect of coupling to neutron-transfer reactions on elastic scattering, CRC calculations were performed. All the input parameters were kept the same as in the DWBA calculations discussed in the previous sections. The results are plotted in Fig. 7 as the dotted curve. Inclusion of the transfer channels reduced significantly the elastic cross section at scattering angles larger than about 60°.

In a series of test calculations it was found that in order to account for this effect and improve the fit to the experimental data the imaginary part of the input ^{6}He + ^{206}Pb effective optical potential had to be modified to be of "short range" form—a Woods-Saxon shape with parameters $W = 50$ MeV, $R = 1.0 \times 206^{1/3}$ fm, and $a = 0.2$ fm. It is interesting to note that the results of the calculations were found to be insensitive to changes in the real part of this potential. If, in addition to the imaginary part of the entrance channel optical potential, the normalization factor S is reduced to a value of 3.6, the results of the calculation describe the elastic scattering data very well (solid curve in Fig. 7).

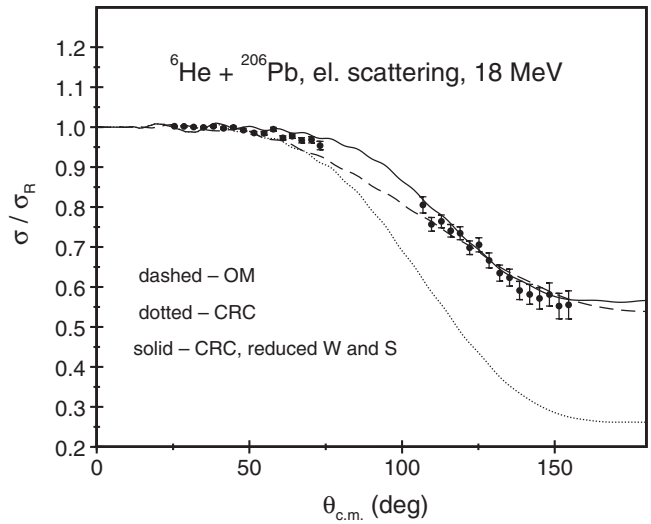

FIG. 7. Effect of neutron-transfer reactions on the elastic scattering studied by means of CRC calculations. The dashed curve shows the optical model calculation from Fig. 5 with the effective potential; the dotted curve shows the CRC calculation with one- and two-neutron transfers included. The results of the latter calculation but with a reduced imaginary potential are plotted as the solid curve.

V. SUMMARY AND CONCLUSIONS

The elastic scattering data could be well reproduced by a CDCC calculation including the effects of ^{6}He breakup only. This is in agreement with previous work on $^{6}\mathrm{He} + {}^{208}\mathrm{Pb}$ elastic scattering at the somewhat higher energy of 22 MeV [11–14]. The present calculations slightly overpredict the data at backward angles, $\theta_{c.m.} \geqslant 125^{\circ}$, whereas the more sophisticated four-body CDCC calculations of Ref. [11] tend to underpredict the elastic scattering cross section in this region. The dynamic polarization potential derived from these calculations has a similar shape to that found for a ^{208}Pb target, with long-range absorption and a long-range attractive real part [13].

Coupled reaction channels calculations based on the effective $^{6}\mathrm{He} + {}^{206}\mathrm{Pb}$ optical potential (bare plus DPP) and including neutron-transfer reactions were also able to describe well elastic scattering after a significant reduction of the imaginary part of the effective potential. This suggests that neutron-transfer reactions are the main processes responsible for the absorption of flux from the elastic channel at this energy and that their role becomes more important at energies below the Coulomb barrier. This is consistent with the CRC calculations of Refs. [28,29] which included $1n$ transfer only. Thus, the inclusion of neutron-transfer processes produces a different effect on elastic scattering compared to that of the inclusion of couplings to the ^{6}He breakup states. The latter modify not only the imaginary part of the effective optical potential but also its real part.

The model calculations overpredict the inclusive α-particle production cross section at forward angles. This could in part be explained by the approximations made in transforming the calculated breakup yield from the c.m. frame to the laboratory frame, although this is unlikely to account for all the discrepancy. At backward angles, the α yield could be explained by two processes: $1n$- and $2n$-transfer reactions. The calculated cross sections for these reactions were of similar order, in contrast to the conclusions drawn previously from analyses of the α yield from the $^{6}\mathrm{He} + {}^{208}\mathrm{Pb}$ interaction, where $2n$ transfer was found to be dominant [3,12,15]. However, we emphasize that the approximate parity in the magnitude of the $1n$- and $2n$-transfer reaction cross sections of the present work is not an experimental result and therefore very much model dependent; in particular, the normalization of the $2n$-transfer cross section is sensitive to the magnitude of the calculated breakup cross section, which is not completely reliable in the simplified model employed here.

In a series of remarkable α-neutron coincidence measurements [30–32] carried out at the TwinSol facility at the University of Notre Dame for the $^{6}\mathrm{He} + {}^{209}\mathrm{Bi}$ system at an incident ^{6}He energy of 22.5 MeV, $2n$ transfer was also found to be the dominant α-particle production mechanism, accounting for approximately 55% of the total α yield, with $1n$ transfer and direct breakup making similar contributions of around 20%–25% each. The experimental ratio of $2n$ to $1n$ transfer is thus about 2.5 in this system. Later triple-coincidence measurements between α particles, neutrons, and characteristic γ rays of the targetlike residues for the $^{6}\mathrm{He} + {}^{65}\mathrm{Cu}$ system [33] at a much higher energy relative to the relevant Coulomb barrier revealed a measured ratio of $2n$ to $1n$ transfer of around 10, suggesting that the trade-off between the two transfer mechanisms is strongly target and/or energy dependent.

The DWBA calculations of Sec. IV give a $2n$- to $1n$-transfer ratio of about 1.4, much lower than the experimental value for the $^{6}\mathrm{He} + {}^{209}\mathrm{Bi}$ system at a similar energy. This discrepancy could possibly be explained as due to dependence on incident energy and target structure. The incident energies are quite close (the difference in Coulomb barrier for ^{206}Pb and ^{209}Bi targets being negligible here) but in this region the $1n$-transfer cross section changes rather rapidly as a function of incident energy; in the calculations presented in Fig. 14 of Ref. [34] the $1n$-transfer cross section for the $^{6}\mathrm{He} + {}^{208}\mathrm{Pb}$ system at $E_{\mathrm{lab}} = 22$ MeV is about 2.5 times larger than that at 18 MeV. However, if this is to explain the larger importance of $1n$ transfer at the lower energy that our calculations suggest it would require the $2n$-transfer cross section to drop off even more rapidly as the incident energy is decreased. The results of Ref. [3] suggest that this is not the case. Regarding the influence of target structure, since the $2n$ transfer populates states close to or in the target + $2n$ continuum we would expect little target-specific variation in the $2n$-transfer cross section for targets so close in mass and charge, and likewise for the direct breakup where the target is essentially a spectator. Of the α-particle production mechanisms, $1n$ transfer is likely to be the most sensitive to target structure influences since it populates known low-lying single-neutron levels in the targetlike residual nucleus. In this case, however, we would expect the $1n$-transfer cross section for a ^{208}Pb target to be largest and that for ^{209}Bi smallest, with ^{206}Pb somewhere in between. Since this does not appear to be the case, it is most likely that the model adopted for the $2n$ transfer in this work is too simplified and underestimates the $2n$-transfer contribution to the total α yield.

Finally, in this work we have considered breakup and $2n$ transfer as two distinct processes modeled by CDCC and

by DWBA and CRC, respectively. However, as pointed out in Refs. [15,35] for example, breakup may be modeled as "transfer to the continuum" provided sufficient partial waves are included in the $2n$-target relative motion. Nevertheless, given the forward-peaked nature of the calculated CDCC breakup cross section it is difficult to image how $2n$ transfer could produce such a shape in the angular distribution at near- and sub-barrier energies on purely kinematic grounds (transfer cross sections at these energies being markedly backward-peaked). However, the present data for the inclusive α-particle cross section do not exhibit a peak in this angular region; thus it is certainly possible that a fully converged "transfer to the continuum" calculation could reproduce the observed shape of the angular distribution, although it might require very large partial waves in the $2n$-^{206}Pb continuum ($\ell_f > 8\hbar$) to do so (see Ref. [15]). It is also possible that the lack of a forward-angle peak in the experimental inclusive α-particle angular distribution is due to kinematic "washing out" of the structure; it will be recalled that the CDCC calculations represent the laboratory frame "^{6}He" inelastic scattering angular distribution rather than the α-particle distribution. The subsequent decay of the unbound "excited states" of ^{6}He could lead to a spreading out of the breakup peak in the measured α-particle distribution.

On the other hand, CDCC calculations are unable to account for the observed large backward angle α-particle cross sections in the $^6\mathrm{He} + ^{208}\mathrm{Pb}$ system (see, e.g., Ref. [15]). The present calculations for the $^6\mathrm{He} + ^{206}\mathrm{Pb}$ system have a similar problem. While this could possibly be due to lack of complete convergence in the CDCC calculations (since extra partial waves and/or higher momentum bins could be required) this seems somewhat unlikely, again on kinematic grounds; CDCC effectively calculates the "inelastic scattering" of ^{6}He which is naturally forward peaked (although inelastic scattering angular distributions do tend to become "flatter" as a function of angle at sub-barrier energies).

The results reported here suggest that to describe completely the available data for this system both breakup and transfer processes must be included in the calculation. In particular, the $1n$ transfer seems to have a greater importance than suggested by previous work for the $^6\mathrm{He} + ^{208}\mathrm{Pb}$ system. These results also point to the need for a more sophisticated theory to understand completely the reaction mechanisms. The CRC calculations of Ref. [15] still fail to describe all the observed backward angle α-particle strength, pointing to limitations in the simple dineutron model picture. To make further progress in this area a model that treats breakup and $1n$ and $2n$ transfer on an equal footing and which incorporates the experimental indistinguishability of transfer to the nonresonant $2n$ + target continuum and direct breakup to the nonresonant $\alpha + 2n$ continuum is needed.

ACKNOWLEDGMENTS

This work was supported in part by Grant No. FPA2010-22131-C02-01 from the Spanish Ministry of Science.

[1] A. M. Sánchez-Benítez *et al.*, Nucl. Phys. A **803**, 30 (2008).
[2] O. R. Kakuee *et al.*, Nucl. Phys. A **728**, 339 (2003).
[3] D. Escrig *et al.*, Nucl. Phys. A **792**, 2 (2007).
[4] Yu. E. Penionzhkevich, V. I. Zagrebaev, S. M. Lukyanov, and R. Kalpakchieva, Phys. Rev. Lett. **96**, 162701 (2006).
[5] R. Wolski *et al.*, Eur. Phys. J. A **47**, 111 (2011).
[6] J. Vervier, Nucl. Phys. A **616**, 97c (1997).
[7] A. M. Sánchez-Benítez *et al.*, J. Phys. G **31**, S1953 (2005).
[8] O. R. Kakuee, Ph.D. thesis, University of Edinburgh, 2000.
[9] J. Rahighi *et al.*, Nucl. Instrum. Methods Phys. Res. A **578**, 185 (2007).
[10] A. M. Sánchez-Benítez, Ph.D. thesis, University of Huelva, 2005.
[11] M. Rodríguez-Gallardo, J. M. Arias, J. Gomez-Camacho, A. M. Moro, I. J. Thompson, and J. A. Tostevin, Phys. Rev. C **80**, 051601R (2009).
[12] L. Acosta *et al.*, Phys. Rev. C **84**, 044604 (2011).
[13] K. Rusek, Eur. Phys. J. A **41**, 399 (2009).
[14] A. M. Moro, K. Rusek, J. M. Arias, J. Gómez-Camacho, and M. Rodríguez-Gallardo, Phys. Rev. C **75**, 064607 (2007).
[15] J. P. Fernández-Garcia, M. A. G. Alvarez, A. M. Moro, and M. Rodríguez-Gallardo, Phys. Lett. B **693**, 310 (2010).
[16] I. J. Thompson, Comput. Phys. Rep. **7**, 167 (1988).
[17] K. Rusek, K. W. Kemper, and R. Wolski, Phys. Rev. C **64**, 044602 (2001).
[18] K. Rusek, I. Martel, J. Gómez-Camacho, A. M. Moro, and R. Raabe, Phys. Rev. C **72**, 037603 (2005).
[19] K. Rusek, N. Keeley, K. W. Kemper, and R. Raabe, Phys. Rev. C **67**, 041604(R) (2003).
[20] C. M. Perey and F. G. Perey, Phys. Rev. **132**, 755 (1963).
[21] G. Goldring *et al.*, Phys. Lett. B **32**, 465 (1970).
[22] M. A. Franey and P. J. Ellis, Phys. Rev. C **23**, 787 (1981).
[23] I. J. Thompson, M. A. Nagarajan, J. S. Lilley, and M. J. Smithson, Nucl. Phys. A **505**, 84 (1989).
[24] O. F. Nemets *et al.*, *Nucleon Clusters in Atomic Nuclei and Many-Body Transfer Reactions* (Ukrainian Academy of Science, Institute for Nuclear Research, Kiev, 1988) (in Russian).
[25] R. A. Moyer, B. L. Cohen, and R. C. Diehl, Phys. Rev. C **2**, 1898 (1970).
[26] K. Rusek, L. Giot, and P. Roussel-Chomaz, Eur. Phys. J. A **32**, 159 (2007).
[27] R. L. Varner *et al.*, Phys. Rep. **201**, 57 (1991).
[28] N. Keeley, N. Alamanos, K. W. Kemper, and K. Rusek, Prog. Part. Nucl. Phys. **63**, 396 (2009).
[29] N. Keeley and N. Alamanos, Phys. Rev. C **77**, 054602 (2008).
[30] J. P. Bychowski *et al.*, Phys. Lett. B **596**, 26 (2004).
[31] P. A. DeYoung *et al.*, Phys. Rev. C **71**, 051601(R) (2005).
[32] J. J. Kolata *et al.*, Phys. Rev. C **75**, 031302(R) (2007).
[33] A. Chatterjee *et al.*, Phys. Rev. Lett. **101**, 032701 (2008).
[34] N. Keeley, R. Raabe, N. Alamanos, and J. L. Sida, Prog. Part. Nucl. Phys. **59**, 579 (2007).
[35] A. M. Moro and F. M. Nunes, Nucl. Phys. A **767**, 138 (2006).